

Journal of Biomedical Optics

SPIEDigitalLibrary.org/jbo

Time-resolved singlet oxygen luminescence detection under photodynamic therapy relevant conditions: comparison of *ex vivo* application of two photosensitizer formulations

Jan C. Schlothauer
Steffen Hackbarth
Lutz Jäger
Kai Drobniowski
Hemantbhai Patel
Sergiu M. Gorun
Beate Röder

Time-resolved singlet oxygen luminescence detection under photodynamic therapy relevant conditions: comparison of *ex vivo* application of two photosensitizer formulations

Jan C. Schlothauer,^a Steffen Hackbarth,^a Lutz Jäger,^a Kai Drobniowski,^a Hemantbhai Patel,^b Sergiu M. Gorun,^b and Beate Röder^a

^aHumboldt-Universität zu Berlin, Institute of Physics, Newtonstr. 15, 12489 Berlin, Germany

^bSeton Hall University, Department of Chemistry and Biochemistry, 400 South Orange Avenue, South Orange, New Jersey 07079

Abstract. Singlet oxygen plays a crucial role in photo-dermatology and photodynamic therapy (PDT) of cancer. Its direct observation by measuring the phosphorescence at 1270 nm, however, is still challenging due to the very low emission probability. It is especially challenging for the time-resolved detection of singlet oxygen kinetics *in vivo* which is of special interest for biomedical applications. Photosensitized generation of singlet oxygen, in pig ear skin as model for human skin, is investigated here. Two photosensitizers (PS) were topically applied to the pig ear skin and examined in a comparative study, which include the amphiphilic pheophorbide-a and the highly hydrophobic perfluoroalkylated zinc phthalocyanine (F₆₄PcZn). Fluorescence microscopy indicates the exclusive accumulation of pheophorbide-a in the stratum corneum, while F₆₄PcZn can also accumulate in deeper layers of the epidermis of the pig ear skin. The kinetics obtained with phosphorescence measurements show the singlet oxygen interaction with the PS microenvironment. Different generation sites of singlet oxygen correlate with the luminescence kinetics. The results show that singlet oxygen luminescence detection can be used as a diagnostic tool, not only for research, but also during treatment. The detection methodology is suitable for the monitoring of chemical quenchers' oxidation as well as O₂ saturation at singlet oxygen concentration levels relevant to PDT treatment protocols. © 2012 Society of Photo-Optical Instrumentation Engineers (SPIE). [DOI: 10.1117/1.JBO.17.11.115005]

Keywords: singlet oxygen; time-resolved singlet oxygen luminescence; *ex vivo*; skin models; intracellular lipids; photodynamic therapy.

Paper 12364P received Jun. 11, 2012; revised manuscript received Oct. 8, 2012; accepted for publication Oct. 15, 2012; published online Nov. 8, 2012.

1 Introduction

The majority of living organisms on Earth utilize oxygen for respiration and energy conversion. Molecular oxygen in its lowest excited electronic state, singlet oxygen [¹O₂], is a highly reactive species generated spontaneously *in vivo* upon exposure of endogenous photosensitizers (PS), such as flavins, to ultraviolet to visible radiation.¹⁻³ ¹O₂ is involved in many chemical and biological processes such as signal transduction for the expression of several proteins, gene regulation via the transcription factor activator protein-2 as well as activation of protein kinases.⁴⁻⁶ Moreover, ¹O₂ is identified as one of the main factors contributing to skin aging and skin cancer.^{7,8}

Photodynamic therapy (PDT) exploits the photosensitized generation of ¹O₂. The administration of a PS to a patient followed by localized light (red or near infrared) exposure, for example of malignant tissue, results in damage to the cancer cells. This therapy is quite selective since the PS and the low energy light are not toxic by themselves. They generate the toxic effect only if present simultaneously and advantageously at the selected location of the targeted tissue. Neighboring, healthy tissue that is not illuminated is not damaged.⁹⁻¹¹

The distribution of PSs in biological environments and their ability to generate ¹O₂ are features critically important for PDT

applications. The electronic and structural parameters that determine distribution properties can be determined via classical chemical and physical methods, while the methodologies of ¹O₂ detection *in vitro* and *in vivo* are subjects to continuous improvements.¹² The evaluation of the efficiency of novel PSs could benefit greatly from *in vivo* time-resolved ¹O₂ detection and, when applicable, *in situ* will greatly improve PDT treatments.

Singlet oxygen detection, even *in vitro*, often relies on indirect methods. For example, the time-dependent concentration variation of ¹O₂ quenchers such as uric acid or dichlorofluorescein diacetate.^{7,13} The reliability of indirect methods, however, is poor in inhomogeneous systems such as biological samples. Specifically, the ¹O₂ diffusion in cells is limited by its lifetime to less than 0.3 μm, a distance which is at most as large as the dimension of some cell organelles.¹⁴⁻¹⁷ Consequently, the accumulation loci of the quencher, presumably present throughout organelles, may exceed the ¹O₂ diffusion area which leaves a fraction of the quencher out of ¹O₂ reach. Since the quencher and PS may have different distribution patterns, no reliable information can be gained from indirect measurements. Thus, using such reporter substances in skin *in vivo* is difficult or impossible.¹ Singlet oxygen measurements *in vivo* are even more difficult. Indirect methods, such as ESR detection of nitroxyl spin probes are common.¹⁸ Fluorescence microscopy

Address all correspondence to: Beate Röder, Humboldt-Universität zu Berlin, Institute of Physics, Germany. E-mail: roeder@physik.hu-berlin.de

0091-3286/2012/\$25.00 © 2012 SPIE

using a fluorescent probe, for example singlet oxygen sensor green, has been applied.¹⁹ Even though this would be a convenient method, results obtained have limited value due to a variety of side effects that may occur, especially in mammalian cells.²⁰ Furthermore, a major limitation of indirect methods is the inability to resolve kinetics. Thus, little information about the environment where the $^1\text{O}_2$ is generated can be gained due to the fact that only the total amount of $^1\text{O}_2$ that has reacted with the probe is measured.

A similar drawback affects direct measurement techniques that track only the total amount of $^1\text{O}_2$ without time resolution.^{11,21} Imaging techniques, with a resolution on the order of millimeters, have been applied *in vivo* using scanning techniques or a camera.^{22,23} Using these methods, approaches have also tracked only the total amount of $^1\text{O}_2$ luminescence intensity is observed without time resolution. The direct approach of time-resolved $^1\text{O}_2$ detection is usually based on detection of the characteristic luminescence at around 1270 nm.²⁴ Despite the low quantum yield and consequent low-intensity, luminescence-based measurements have been pursued intensely. Recently, the detection of $^1\text{O}_2$ luminescence kinetics, from cells in suspension as well as from single cells under a microscope, has become possible.^{11,16,17,21,25} Using an innovative technological approach, Lee et al. measured the $^1\text{O}_2$ decay time-resolved after excitation of a PS with a microsecond light pulse. This way, short rise times of the luminescence signal cannot be usually resolved, as illustrated in Sec. 2.1.²⁶ In some heterogeneous systems, such as biological cells, this short luminescence rise time is determined by the $^1\text{O}_2$ decay time.²⁷ Using laser excitation in the nanosecond regime, direct, time-resolved measurements of $^1\text{O}_2$ *in vivo* on rats, photosensitized by systemic drug administration, have been reported, yet the low signal-to-noise ratio limited the ability to determine the kinetics accurately.¹¹ In the best case thus far, the direct, time-resolved measurements of $^1\text{O}_2$ in skin generated by UVA laser excitation at 355 nm irradiation of endogenous PSs, yielded a weak and complex signal where semi-quantified decay time components were attributed. These time components include a time below 2 μs , a decay of 8 μs fitted to the luminescence signal in the time region from 2 to 16 μs , and a long lived decay time greater than 16 μs .²⁵ Time-resolved $^1\text{O}_2$ luminescence measurements *in vivo* are still very difficult and require refinement to provide a diagnostic tool for use in clinical protocols or research.¹

Recently, we reported an experimental set-up with very high sensitivity that allows the use of low illumination doses. This facilitated the discovery that, in the case of cells in suspension, the $^1\text{O}_2$ and PS triplet decay times are a function of light exposure.^{28,29} Additionally, the SNR of the signals of $^1\text{O}_2$, generated in membranous systems, is sufficiently high to allow distinguishing homogenous environments from heterogeneous, membranous systems by evaluating the kinetics of $^1\text{O}_2$ luminescence.²⁷

Here, we report the comparative investigation of two PSs applied to pig ear skin. Pig ear skin *ex vivo* is considered a good model for human skin in various aspects.³⁰ The time-resolved $^1\text{O}_2$ luminescence measurements provide insight into the interactions of the PS with its environment. In conjunction with additional spectroscopic measurements, we show that significant differences in the accumulation of the two PSs can consistently be observed in the $^1\text{O}_2$ luminescence kinetics. This methodology also allows tracking the oxidation of chemical quenchers and O_2 saturation.

2 Materials and Methods

2.1 Photosensitizers

Pheophorbide-a (Pheo), Fig. 1(a), a dye initially extracted from leaves of *Urtica urens*, was obtained from spirulina *Arthrospira platensis*.³¹ 1,4,8,11,15,18,22,25-octakis-fluoro-2,3,9,10,16,17,23,24-octakis-perfluoro(isopropyl)phthalocyanine zinc (F_{64}PcZn), Fig. 1(b), was prepared using a microwave assisted procedure.³² For the PS in an oxygen containing environment, the fluorescence intensity is correlated to the $^1\text{O}_2$ quantum yield.³³ Therefore, in the investigated samples, the localization pattern determined with fluorescence microscopy equals that of $^1\text{O}_2$ generation.

2.2 Sample Preparation and Handling

Physiogel® hypoallergen vanishing crème was obtained from Stiefel Laboratorium GmbH, Germany. Pheo was suspended in Physiogel® (0.1% by weight) to yield a molar concentration of $1.7 \cdot 10^{-3}$ M. For the F_{64}PcZn : crème composition, a ratio of 3.5:1 mg:ml was used to yield the same molar concentration.

Thin layers of the crème mixtures were placed on glass slides for experiments involving only the PS in the crème. The crème itself exhibited no luminescence in the spectral region of $^1\text{O}_2$ phosphorescence.

Pig ear skin samples, from animals sacrificed the previous day, were obtained from the Dermatological Clinic, Charité Hospital, Berlin, Germany. The ears were washed and the hair was removed using a razorblade or scalpel. Samples from the ear were cut out. On these skin samples, the crème was applied, topically, without exertion of any force at an amount of approximately 20 to 40 mg/cm². Residual (not absorbed) crème was removed from the skin surface after 60 min by washing the sample with water.

Lipids were extracted by separating a peripheral epidermal layer from the skin, drying them, and then extracting them with petroleum ether.³⁴ No further action was taken to ensure isolation of only the stratum corneum. Fatty tissue from lower layers was also washed with petroleum ether to extract the lipids. The solvent was removed and the lipid residues were re-suspended in solutions of the PS in dichloromethane (DCM). Following homogenization, the mixture was evaporated on glass slides to yield lipid films which are used for spectroscopic measurements. The area of the lipid film was chosen to be equal to the skin area used for lipid extraction. The amount of PS in the lipid

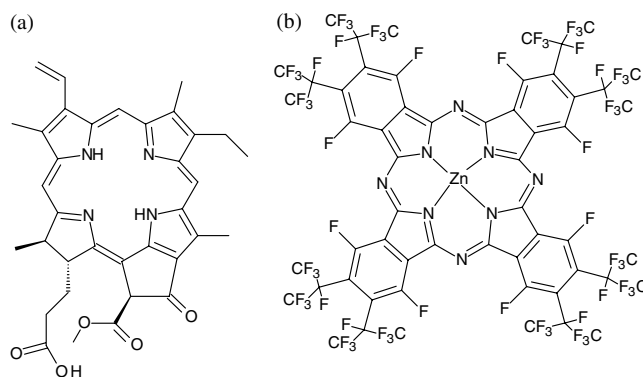


Fig. 1 Molecular structures of the photosensitizers. (a) Pheophorbide-a (Pheo); (b) 1,4,8,11,15,18,22,25-octakis-fluoro-2,3,9,10,16,17,23,24-octakis-perfluoro(isopropyl)phthalocyanine zinc (F_{64}PcZn);

film was chosen a factor of 20 less than the amount applied in crème to the same area. Due to inhomogeneity of the lipid film and uncertainties of the crème application, these values have estimated errors in the order of a factor of 2 to 4. The residue left after washing stratum corneum layers was ground into a mortar along with a solution of PS in DCM. The keratinous residue, obtained after the evaporation of DCM, was placed on adhesive tape in order to fix its position. The tape was shown not to interfere with $^1\text{O}_2$ measurements. The epidermis of the samples, used for the biopsies in Fig. 2, was impaired by stripping once with adhesive tape with cyanoacrylate before application of the PS. The procedure was similar to common tape stripping used in dermatology, described in Ref. 35. All samples were handled in almost total darkness by using only low intensity light of wavelengths not absorbed by the PS.

2.3 Singlet Oxygen Kinetics Methodology

The time-dependency, $^1\text{O}_2(t)$, of the amount of PS-generated $^1\text{O}_2$ in a homogeneous environment is simplified described by Eq. (1):

$$^1\text{O}_2(t) = \frac{C}{\tau_T - \tau_D} (e^{-t/\tau_T} - e^{-t/\tau_D}). \quad (1)$$

Considering a microsecond time scale, the PS molecules can be assumed to reach the triplet state instantaneously following a nanosecond laser pulse excitation. The fitting constant C accounts for the number of initially excited PS molecules, while τ_D and τ_T represent the $^1\text{O}_2$ and PS triplet state decay times, respectively. The sign of the preexponential factor can change depending on the relative values of the two decay times. A signal rise is determined mainly by the faster process the decay by the slower one.²⁵ Hence, the firm assignment of PS triplet and $^1\text{O}_2$ decay times to the fitting parameters of the luminescence signal requires additional experiments.¹² The PS triplet lifetime can be determined directly by flash photolysis or indirectly by the addition of quenchers in variable concentrations followed by the monitoring of the changes in $^1\text{O}_2$ decay time.³⁶ Considering the high $^1\text{O}_2$ quantum yields, the PS triplet decay time is mainly determined by the efficiency of the energy transfer to O_2 . Thus, reducing the O_2 concentration leads to an increased PS triplet decay time while the $^1\text{O}_2$ decay time remains constant allowing a quantitative differentiation between the two processes and assigning of τ_D and τ_T to the fitted parameters.³⁷

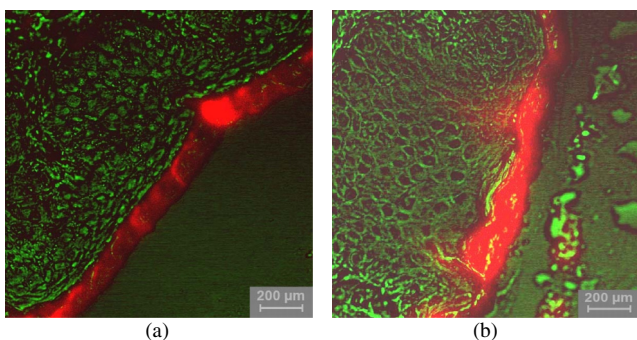


Fig. 2 Fluorescence microscopy image of skin samples prepared with the photosensitizer-crème according to Sec. 2. The Photosensitizer is (a) Pheo and (b) F_{64}PcZn . Pheo shows fluorescence only in the stratum corneum while F_{64}PcZn is also fluorescing in deeper layers of the epidermis.

It must be noted, that Eq. (1) is applicable only for homogeneous environments. In a first approximation, this model can be extended to heterogeneous systems comprising a number of homogeneous environments, therefore, neglecting the cross-diffusion between them. A sum of two (or more) distinct homogeneous environments, each described by Eq. (1), is then fitted to the data.²⁴ The consideration of such multiple environments results in the determination of more accurate fit parameters if the geometry of the system is known.^{27,38}

2.4 Singlet Oxygen Luminescence Detection: Time Correlated Multiphoton Counting

The excitation source comprised a frequency-doubled diode pumped Nd^{3+} -YAG laser and a customized dye laser. The light intensity, adjustable up to 20 mW average power, was maintained at 5 mW, measured with a LabMax/J 10MT- 10 kHz, (Coherent). The repetition rate of 12.2 kHz resulted in approx. 0.4 μJ pulse energy. Due to the shape of the laser beam, the intensity at the sample is approx. 50 mW/cm^2 . The acquisition time for a single measurement was 20 s, thus, one measurement delivers approximately 1 J/cm^2 to the sample. The excitation wavelength was chosen to match the absorption maximum of the lowest energy absorption band of the PS. For Pheo, excitation was done at 666 nm, for F_{64}PcZn at 683 nm.

Luminescence was detected with a photomultiplier H-10330-45 (HAMAMATSU Germany) that sensitive from 950 to 1400 nm with quantum efficiency of 2%. An $f = 0.6$ lens transfers collimated light onto the effective area of the anode (1.6 mm diameter). The rise-time of 900 ps and the transit time spread of 300 ps may be neglected in the $^1\text{O}_2$ luminescence decay time domain. The high sensitivity of the setup not only allows the detection of $^1\text{O}_2$, but also the determination of rise and decay times with an accuracy and reproducibility of 0.1 μs in many biological samples. If larger error margins are given for absolute values, these are due to sample variance. The evolution of the luminescence signal function of on-going illumination was performed via repeated measurement cycles at constant time intervals, as reported previously.^{27–29}

Since the $^1\text{O}_2$ luminescence emission is centred at 1270 nm, an interference filter, with a central wavelength at 1270 nm, was used to discriminate other emission. The fact that $^1\text{O}_2$ is the source of the luminescence signals reported here was verified by spectral analysis of the signal. For this investigation, the luminescence was recorded using interference filters with central wavelengths at 1200, 1250, and 1300 nm. The intensities of these signals were compared to the signal obtained with the interference filter centered at 1270. A clear intensity maximum at 1270 nm is observed with no signal contribution at 1200 nm, verifying $^1\text{O}_2$ as source of the luminescence (data not shown).

2.5 Flash Photolysis Measurements

An ns- Nd^{3+} -YAG pumped OPO (Ekspla, 420 to 2500 nm) laser was used for excitation. Excitation energy was 2 mJ in a 10 ns pulse at a repetition rate of 10 Hz. A stabilized light emitting diode (LED) was used as probe light source. Time dependent, transient triplet-triplet absorption spectra were observed perpendicular to the excitation with a band pass interference filter selected the transient absorption wavelength. The transmitted light was detected using a Si-photodiode with an integrated fast preamplifier (Elektronik Manufaktur Mahlsdorf, EMM, Berlin) using a recording oscilloscope (HP5415). The setup

allows the determination of PS triplet decay times as short as $0.1 \mu\text{s}$.

3 Results and Discussion

Photosensitized generation of $^1\text{O}_2$ in skin poses a highly complex system. To explain the luminescence kinetics of this system in the following, initially, the interaction of the PSs and the photosensitized generated $^1\text{O}_2$ with the carrier crème is elucidated. Secondly, measurement results of skin samples and, finally, measurement results of the components extracted from the skin are discussed.

3.1 Distribution of Photosensitizer Fluorescence in Crème

The suspension of the two PS's in crème was monitored via fluorescence microscopy. Figure 3 reveals that there are significant differences in solubility. Pheo exhibits homogenous fluorescence at room temperature, suggesting a homogeneous distribution, even though the light scattering image clearly shows a structure. The F_{64}PcZn is strongly partitioned in a pattern, which will be referred to as droplets. Incubation of 1 h at 37°C results in the Pheo migration within small droplets. No effect on the distribution of F_{64}PcZn was observed, the size of the droplets was larger at the higher temperature. The high hydrophobicity of F_{64}PcZn explains the exclusive accumulation in the droplets, pointing to the statement: The crème consists of lipid droplets suspended in a water phase.

3.2 Singlet Oxygen Generation in Crème

Both PS-crème compositions exhibit strong photosensitizing activity as judged by the observation of intense $^1\text{O}_2$ luminescence signals, as illustrated in Fig. 4. In contrast to the fluorescence microscopy indicating a homogenous distribution of Pheo and an inhomogeneous distribution of F_{64}PcZn in the crème at room temperature, the $^1\text{O}_2$ luminescence signal for the Pheo-crème sample could not be fit satisfactory with the model for homogenous environments [Fig. 4(a)], however, in the case of F_{64}PcZn -crème, the simplified Eq. (1) for homogenous environments is suitable [Fig. 4(b)].

To fit the luminescence signal of the Pheo-crème at room temperature, we would rather use a model that assumes the distribution of $^1\text{O}_2$ in two different environments within the crème. Fitting the data with this model yields two sets of decay times,

namely $\tau_{1a} = 0.6 \mu\text{s}$ and $\tau_{1b} = 26 \mu\text{s}$ in one environment and $\tau_{2a} = 26 \mu\text{s}$ $\tau_{2b} = 3.5 \mu\text{s}$ in the other. A $^1\text{O}_2$ decay time of $3.5 \mu\text{s}$ is consistent with literature values for the $^1\text{O}_2$ decay time in water.²⁴ This observation is consistent with the statement that the crème is an emulsion in which lipid droplets are surrounded by a water phase. However, this explanation needs to be treated with caution since Pheo aggregates in pure water and neither fluoresces nor generates $^1\text{O}_2$.³⁹ Thus, one cannot assume that Pheo is generating $^1\text{O}_2$ in a pure water phase. Rather, we propose Pheo might be present in a lipid system, which is suspended in the water phase and, thus, Pheo is still able to generate single oxygen. The term lipid, in contrast to lipids, will be used here to distinguish lipids organized in membranous systems such as liposomes or micelles from lipids that do not form these structures and, thus, cannot be suspended in water.

The flash photolysis measurements support this hypothesis. A single PS triplet decay time can be observed, thus, no $^1\text{O}_2$ generation in radically different environments is expected. In consideration of the amphiphilic properties of Pheo, the spontaneous formation of lipoids, which are suspended in the water phase, is likely. It is known, for example, that Pheo can easily be incorporated into lipid structures such as liposomes or micelles where the preparation method is based on self-organized formation of lipoids.⁴⁰

The decay parameter values in Ref. 28 must be placed in the context of the temperature dependence of the Pheo-in-crème system. The $^1\text{O}_2$ luminescence signals of Pheo-crème at 37°C can be fit with the standard double-exponential model, yielding a single decay time of $23 \pm 2 \mu\text{s}$ and a PS triplet time of $\tau_T = 0.8 \pm 0.2 \mu\text{s}$ which indicates a homogenous environment of $^1\text{O}_2$ generation and decay. Considering the size of the droplets visible with fluorescence microscopy [Fig. 4(c) and 4(d)] and the diffusion length of $^1\text{O}_2$, this interpretation is consistent with the experimental data. If $^1\text{O}_2$ is generated only in the lipid droplet and then diffuses out into a water phase, this would affect the kinetics in the investigated crème only in a negligible way. In a completely lipid environment, the diffusion length of $^1\text{O}_2$ would be in the order of 100 nm .⁴¹ The average droplet size of $5 \mu\text{m}$ is large compared to 100 nm diffusion length of $^1\text{O}_2$. Taking 100 nm as upper limit of the diffusion length for the water phase and a sphere with a diameter of $5 \mu\text{m}$ as the droplet size, a maximum of the $^1\text{O}_2$ generated within a droplet can leave the droplet and be quenched outside. Thus, the observed formation of droplets should have a negligible influence on the $^1\text{O}_2$ kinetics. The kinetics shown in Fig. 4(a) (red) and 4(b) deviate negligibly from the kinetics of a homogenous environment.

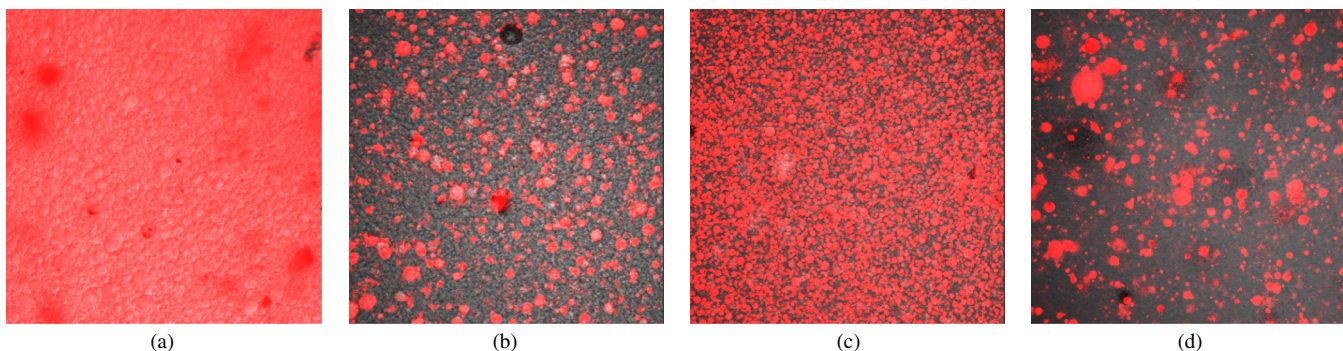


Fig. 3 Fluorescence microscopy images of emulsified photosensitizers. The images are an overlay of the scattered light (black and white) and the PS fluorescence (red). The displayed areas have the approximate dimensions $200 \times 200 \mu\text{m}^2$. (a) Pheophorbide-a at room temperature; (b) F_{64}PcZn at room temperature; (c) pheophorbide-a after incubation at 37°C ; and (d) F_{64}PcZn after incubation at 37°C .

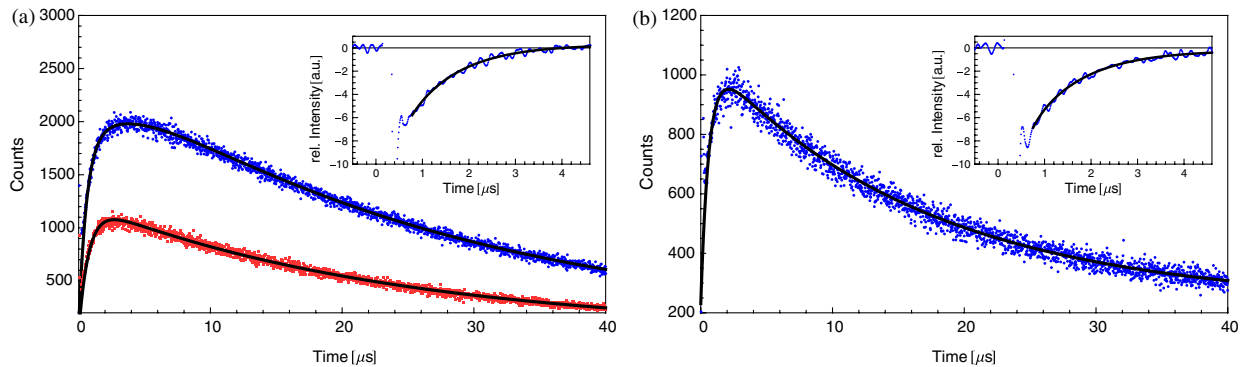


Fig. 4 Luminescence decay of singlet oxygen photosensitized generated by (a) Pheo and (b) $F_{64}PcZn$ in vanishing crème. Black lines are the fitting curves. (a) Dark Blue dots: measurement at 25°C; Light Red squares: measurement at 37°C. Fitted parameters: (a) 25°C: $\tau_T = 0.6 \pm 0.2 \mu s$, $\tau_{O2a}: 26 \pm 2 \mu s$, $\tau_{O2b}: 3.5 \pm 0.5 \mu s$; 37°C: $\tau_T = 0.8 \pm 0.2 \mu s$, $\tau_{O2}: 23 \pm 2 \mu s$. (b) $\tau_T = 0.6 \pm 0.2 \mu s$, $\tau_{O2}: 17 \pm 2 \mu s$. Insets: Flash photolysis measurements of triplet decay times (a) $\tau_T = 1.1 \pm 0.2 \mu s$ (25°C) (b) $\tau_T = 1.0 \pm 0.2 \mu s$. See the text for details.

This does not justify the use of more complex fitting models. The influence of diffusion on 1O_2 luminescence kinetics have been examined in detail in Ref. 27 for cell suspensions. However, we refrain from further investigating the crème system here as it is only used as a carrier for the PS and not further related to the discussion of the 1O_2 luminescence kinetics of the skin samples.

The decay parameters of 1O_2 luminescence were assigned to the 1O_2 and PS triplet decay times with the help of flash photolysis measurements. The values for the PS triplet decay time are $1.0 \pm 0.2 \mu s$ for Pheo and $1.1 \pm 0.2 \mu s$ for $F_{64}PcZn$ (Fig. 4, insets). The assignments of $\tau_T = 0.6 \pm 0.2 \mu s$ for Pheo and $F_{64}PcZn$ are in accordance with the notion that the shorter time reflects the PS triplet decay. The flash photolysis measurement yields longer PS triplet decay times here, compared to those obtained via 1O_2 luminescence measurement. This may reflect the fact that the pulse energy for a flash photolysis measurement is much higher than for the 1O_2 measurement. Singlet oxygen measurements are done using a laser with a repetition rate of 12.2 kHz and 0.4 μJ energy per pulse. The flash photolysis uses a laser with 10 Hz repetition rate and 10 ns pulse length with energy of 1 mJ. The comparably higher pulse energy may lead to local oxygen depletion which results in a longer PS triplet decay time.

It is interesting to note that, unlike the case of Pheo, protons attached to the nitrogen atoms of the inner ring of the $F_{64}PcZn$ scaffold exhibit a high acidity. This effect also enhances the Lewis acidity of coordinated metal centers, including the Zn^{2+} of $F_{64}PcZn$, which was shown to coordinate ligands exhibiting electron lone pairs such as oxygen of acetone, methanol and even water.⁴² Considering the strong hydrophobic nature of the fluoro groups of the $F_{64}PcZn$, it is not surprising that it is easily soluble in organic solvents including polar alcohols and acetone. The high hydrophobicity causes a binding constant to liposomes (formed by amphiphilic lipoids) smaller than $0.1 (mg/ml)^{-1}$.⁴³ The results shown in Fig. 3, however, indicate favorable solubility in lipids, probably neutral fats or fatty acids not forming a highly structured distribution such as membrane-like structures. This result can be understood considering the overall hydrophobicity of $F_{64}PcZn$ scaffold and the neutral nature of lipids. In contrast, membranes are more amphiphilic in nature due to their lipid components. From a PS materials point of view, the above mentioned properties of $F_{64}PcZn$ suggest that other scaffolds bearing perfluoroalkyl groups might

also exhibit favorable PDT properties in case no accumulation in cells is needed.

3.3 Distribution of Photosensitizer Fluorescence in Skin

The localization of PSs within skin samples was investigated using fluorescence microscopy, as shown in Fig. 2. Pheo is localized exclusively in the stratum corneum, as shown in Fig. 4. Pheo was applied after the stratum corneum barrier was disrupted by tape stripping, nevertheless, no fluorescence in deeper epidermal layers is observed. In contrast, $F_{64}PcZn$ fluoresces not only in the stratum corneum, but also in the deeper layers of the epidermis. The ultrastructure of the stratum corneum cannot be resolved using fluorescence microscopy. In order to investigate a possible influence of temperature upon partition effects, pig ears were stored after application of crème both at 37°C and at room temperature. Differences in the localization within the epidermis, depending on the temperature, have not been observed in the skin samples.

3.4 Singlet Oxygen Generation in Ex Vivo Pig Skin

The time-dependent luminescence signals of 1O_2 generated by the two PSs are shown in Fig. 5. Similar to the measurements for cells *in vitro*, reported previously,²⁷ a change of the luminescence kinetics with illumination is observed here. The blue and red curves in Fig. 5 show the initial data and a postillumination measurement, respectively.

Specifically, in the Pheo PS case shown in Fig. 5(a), the PS triplet decay time of the first measurement is $0.3 \pm 0.2 \mu s$ and increases after an illumination of the sample with $5.5 J/cm^2$ to $0.9 \pm 0.2 \mu s$, while the 1O_2 decay time increases from $12.5 \pm 0.5 \mu s$ to $16.7 \pm 0.5 \mu s$. Figure 5(b) shows that $F_{64}PcZn$ is characterized by a similar behavior, with slightly different parameters, suggesting a slower evolution of decay times with illumination. The decay times of the $F_{64}PcZn$ sample increase from $\tau_T = 0.4 \pm 0.2 \mu s$ and $\tau_{O2} = 10.2 \pm 0.5 \mu s$ to $\tau_T = 0.8 \pm 0.2 \mu s$ and $\tau_{O2} = 15.0 \pm 0.5 \mu s$ after delivery of $11 J/cm^2$. This discrepancy could be attributed to the distributions and accumulation of the two PSs in different microenvironments. The amplitude difference of a factor of about 2 to 3 is insufficient for deriving further conclusions about the efficiency of 1O_2 generation as this parameter is subject to a high, sample-dependent variance. The stated errors for the decay time

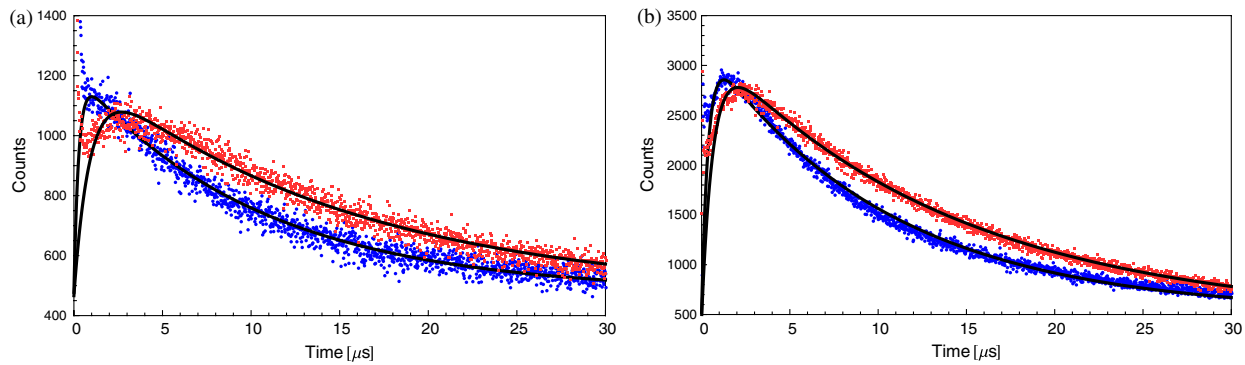


Fig. 5 Luminescence decay of singlet oxygen photosensitized generated by (a) Pheo and (b) $F_{64}PcZn$ in pig skin. Dark Blue dots: initial measurement (1.1 J/cm^2), Light Red squares: measurement after (a) 5.5 J/cm^2 resp. (b) 11 J/cm^2 . Black lines are the fitting curves. Fitted parameters (a) (1.1 J/cm^2): $\tau_T = 0.3 \pm 0.2 \text{ } \mu\text{s}$, $\tau_{O_2} = 12.5 \pm 0.5 \text{ } \mu\text{s}$, (5.5 J/cm^2): $\tau_T = 0.9 \pm 0.2 \text{ } \mu\text{s}$, $\tau_{O_2} = 16.7 \pm 0.5 \text{ } \mu\text{s}$, (b) (1.1 J/cm^2): $\tau_T = 0.4 \pm 0.2 \text{ } \mu\text{s}$, $\tau_{O_2} = 10.2 \pm 0.5 \text{ } \mu\text{s}$, (11 J/cm^2): $\tau_T = 0.8 \pm 0.2 \text{ } \mu\text{s}$, $\tau_{O_2} = 15.0 \pm 0.5 \text{ } \mu\text{s}$.

parameters include sample variability and exhibit a lower relative variance.

The initial 1O_2 decay times for fresh samples of Pheo, $12.5 \text{ } \mu\text{s}$ and $F_{64}PcZn$, $10.2 \text{ } \mu\text{s}$, are about half of those observed in the vanishing crème alone ($26 \text{ } \mu\text{s}$ for Pheo and $17 \text{ } \mu\text{s}$ for $F_{64}PcZn$). The significant reduction indicates a strong interaction between the PS and the stratum corneum. The applicability of the fitting procedure, for homogenous environments, supports the notion that no residual crème remained on the skin during the measurements as the crème's high 1O_2 luminescence signal would show up as a second component of the luminescence signal with different parameters. Small deviations between the fit and the data remain, especially for the $F_{64}PcZn$ sample. This will be discussed below. Yet, the deviations are too small to justify the introduction of a different theoretical model at this moment. In addition the scattering signal, specific for 1O_2 luminescence measurements, cannot be theoretically modeled and is overlapping the luminescence shortly after the laser pulse.¹²

The systematic change in the 1O_2 luminescence signal, as function of the illumination, has been tracked up to a total dose of 20 J/cm^2 , as illustrated in Fig. 6. For both PSs, the triplet decay times initially rise fast and then remain fairly constant after illumination with 10 J/cm^2 . The variation of the PS triplet decay time is attributed to initial oxygen retention within the sample that yields a very short PS triplet decay time at the beginning of the measurement followed by the consumption of oxygen within the skin by chemical reactions. A lower oxygen

concentration is reducing the efficiency of the energy transfer from the PS triplet state to oxygen, a process that is proportional to the oxygen concentration. Consequently, the PS triplet decay time increases and equilibrium is reached when the rate of oxygen diffusion from the environment equals the rate of its local consumption.

A significant difference between Pheo and $F_{64}PcZn$ is observed not only in the kinetics of a single measurement, but also in the change of the 1O_2 decay time with illumination. While, in the Pheo case, the decay time initially rises fast, the 1O_2 decay time of the $F_{64}PcZn$ sample shows a smoother increase with illumination. In biological system, the increasing 1O_2 decay time can be associated with a consumption of chemical quenchers.²⁷ As 1O_2 is generated, it reacts with chemical quenchers such as endogenous antioxidants, proteins, unsaturated lipids, or other oxidative targets occurring in the skin. Since the chemical reaction rate should be proportional to the number of free reaction sites, one would expect their exponential decrease. Practically all major components of the skin such as keratins, proteins, lipids and several antioxidants are known to react with oxygen.^{44,45} A preliminary elucidation of the localization within the ultrastructure of the stratum corneum follows at the end of this section.

Control experiments were performed by saturating samples with N_2 in order to verify the signal origin and parameter assignments of the observed luminescence, as shown in Fig. 7 as in Ref. 28. Purging oxygen by pure N_2 followed by the admission

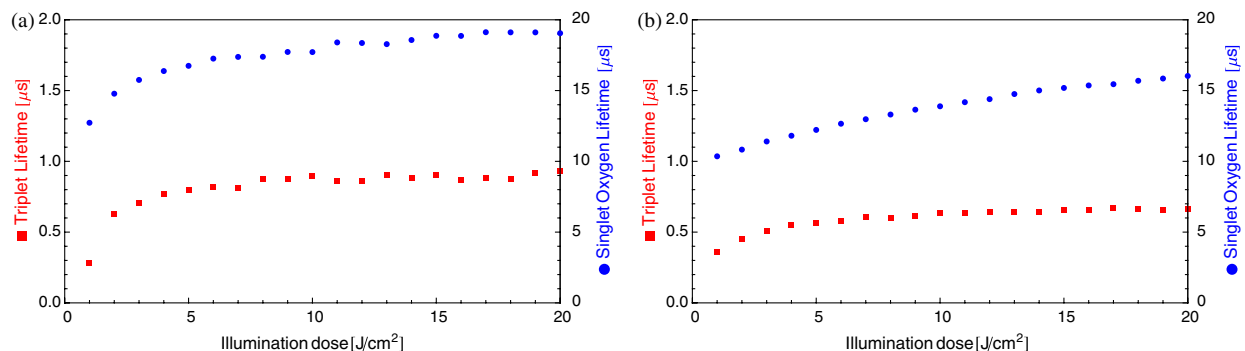


Fig. 6 Variation of 1O_2 and Pheo triplet decay times in pig ear skin as a function of light doses (the scale is proportional to a time scale of 0 to 7 min). The Photosensitizer is (a) Pheo and (b) $F_{64}PcZn$. Fitted parameters: (a) initial measurement (1.1 J/cm^2): $\tau_T = 0.3 \pm 0.2 \text{ } \mu\text{s}$, $\tau_{O_2} = 12.5 \pm 0.5 \text{ } \mu\text{s}$; final measurement (20 J/cm^2): $\tau_T = 0.9 \pm 0.2 \text{ } \mu\text{s}$, $\tau_{O_2} = 19.2 \pm 0.5 \text{ } \mu\text{s}$. (b) initial measurement (1.1 J/cm^2): $\tau_T = 0.4 \pm 0.2 \text{ } \mu\text{s}$, $\tau_{O_2} = 10.2 \pm 0.5 \text{ } \mu\text{s}$; final measurement (20 J/cm^2): $\tau_T = 0.6 \pm 0.2 \text{ } \mu\text{s}$, $\tau_{O_2} = 16.1 \pm 0.5 \text{ } \mu\text{s}$.

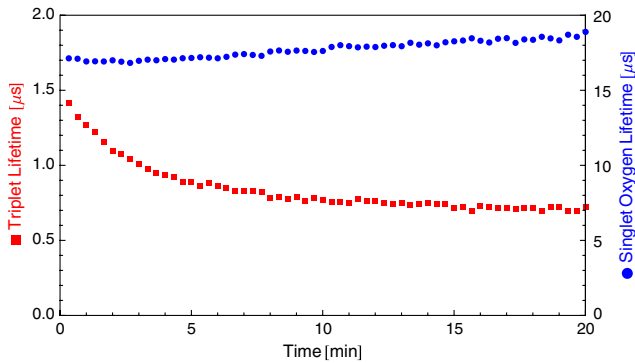


Fig. 7 Change of singlet oxygen and photosensitizer triplet decay time of a pig-ear skin sample prepared with photosensitizer in crème. O_2 was purged by flushing the sample chamber with N_2 . At the beginning of the experiment air was allowed to re-enter the sample. The singlet oxygen time remains fairly constant, except for a slight increase, the photosensitizer triplet decay time decreases, as expected. See the text for details.

of normal air into the sample results in the recovery of the 1270 nm luminescence signal, which was not observed under N_2 . This is the expected behavior if external oxygen is the sole source of the luminescence emission.

The assignments of rise and decay time of the luminescence signal for the skin samples are further verified with this method. Thus, upon allowing normal air to gradually contact the sample following its initial removal with N_2 , the signal recovery exhibits a significant decrease in the rise time as the oxygen level increases, while the longer time remains fairly constant. The increase in oxygen level increases the efficiency of the energy transfer from the PS triplet state to oxygen which results in a lower lifetime of this state. Consequently, the shorter time constant can be unambiguously assigned to the PS triplet decay time. The slight increase of the longer decay time follows the general tendency of the 1O_2 decay time to increase with the illumination dose.

It can be noted, that a self-quenching effect of 1O_2 by molecular (triplet) oxygen has been reported, which might quantitatively affect the decay times.⁴⁶ However, this is negligible here: Considering the variation of both times under N_2/O_2 atmosphere exchange, the assignment made is perspicuous. Since the longer time still increases while the shorter time decreases, the shorter time must be the triplet decay time of the PS. This assignment is alike for Pheo and $F_{64}PcZn$.

3.5 Singlet Oxygen Generation in Extracted Lipid Components of Pig Ear Skin

Singlet oxygen emission from the lipid films was observed for both PSs in both lipid films, as illustrated in Figs. 8 and 9. Singlet oxygen luminescence measurements of the lipid films from subcutaneous tissue show that these lipids contain oxidative targets as well, as shown in Figs. 8 and 10. The dynamics of the change of 1O_2 and PS triplet decay times in skin (Fig. 6) and in subcutaneous tissue (Fig. 10) are alike the dynamics found in lipid films of stratum corneum lipids (Fig. 9). As in the case of stratum corneum lipids, Pheo exhibits an initially fast rise reaching an inflection point at which the speed of increase slows significantly while, for the $F_{64}PcZn$ sample, the 1O_2 decay time increases more smooth and continues to rise at the end of the measurement. The fact that Pheo is generating 1O_2 from these extracted lipids does not contradict the fact that it accumulates only within the stratum corneum since the amphiphilic Pheo cannot diffuse through it in the intact skin to reach these areas.

A dependence of the decay times on the light dose can be observed in the lipid films of stratum corneum lipids as well. Significant structural differences between the extracted lipid and the lipid system present in skin, however, preclude a detailed analysis of the shape of the luminescence signal. As stated above, the simple bi-exponential model, suitable for homogeneous environments, can be improved for heterogeneous systems if the structure of the system is known. In case of the lipid films investigated here (Fig. 8), the inhomogeneity of the system is indicated by the deviation of the simple model from fit of the data and by the 1O_2 luminescence kinetics. The films, obtained with extracted lipids, clearly do not structurally resemble the native lipids present in the stratum corneum or in deeper tissues.⁴⁷ This investigation, even if limited by employing the simple biexponential model, allows the identification of common chemical reactions of 1O_2 that take place in the stratum corneum and the extracted lipids.

Similar differences in the change of the 1O_2 luminescence kinetics between the Pheo and $F_{64}PcZn$ samples can be noticed in the lipid samples as well as in skin. The rate of change of 1O_2 and PS triplet decay time with illumination is steadier for $F_{64}PcZn$ compared with Pheo. The initial change in decay times for Pheo is rapid, reaching a point of equilibrium or much slower growth. The change in kinetics shown is in the same order-of-magnitude as the change observed in the skin samples which

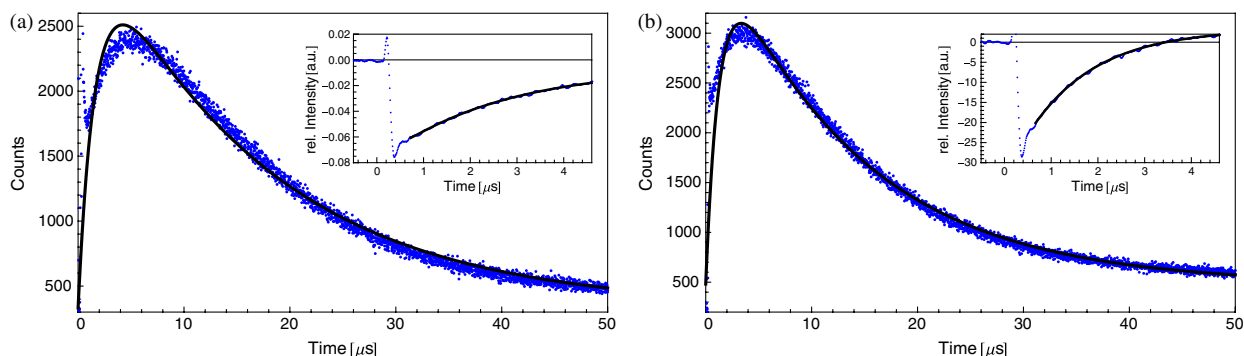


Fig. 8 Luminescence decay of singlet oxygen photosensitized generated by (a) Pheo and (b) $F_{64}PcZn$ in a film of lower tissue lipids. Shown data applies to measurement no. 10 after already illumination with $10 J/cm^2$. Fits were obtained using the biexponential model according to Eq. (1). Fitted parameters: (a) $\tau_T = 2.0 \pm 0.2 \mu s$, $\tau_{O_2} = 16.5 \pm 0.5 \mu s$. (b) $\tau_T = 1.3 \pm 0.2 \mu s$, $\tau_{O_2} = 13.5 \pm 0.5 \mu s$. Insets show flash photolysis measurements conducted after the end of the singlet oxygen measurements. Data was fitted with a single decay time (a) $\tau_1 = 2.5 \pm 0.2 \mu s$ and (b) $1.4 \pm 0.2 \mu s$.

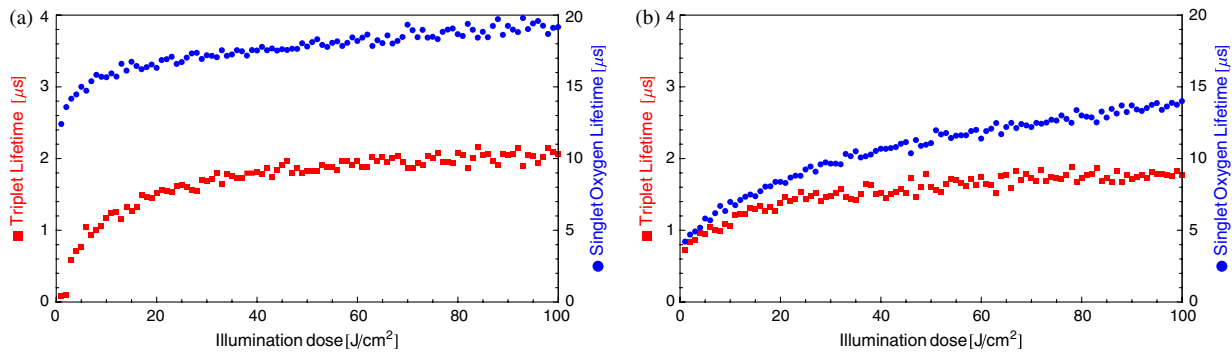


Fig. 9 Variation of singlet oxygen and photosensitizer triplet decay times for (a) Pheo and (b) $F_{64}PcZn$ in a film of stratum corneum lipids as a function of light dose. Fitted parameters: a) initial measurement: $\tau_T = 0.5 \pm 0.2 \mu s$, $\tau_{O_2} = 8 \pm 0.5 \mu s$, final measurement (20 J/cm^2): $\tau_T = 1.9 \pm 0.2 \mu s$, $\tau_{O_2} = 18 \pm 0.5 \mu s$. b) initial measurement $\tau_T = 0.4 \pm 0.2 \mu s$, $\tau_{O_2} = 4 \pm 0.5 \mu s$, final measurement: $\tau_T = 1.8 \pm 0.2 \mu s$, $\tau_{O_2} = 13 \pm 0.5 \mu s$.

indicates the PS and lipid concentrations used for preparing the lipid films closely resemble those in the pig ear.

Since Pheo and $F_{64}PcZn$ are present in equimolar concentrations in the lipid film, the different change in kinetics should not be attributed solely to possible differences in absorption or a lower 1O_2 generation. As indicated already by the measurements in crème and as it can be assumed due to the properties of the PS, we rather propose that this difference in change of kinetics is related to the microenvironment of the PS. Thus, the PS triplet decay time equilibrium values of $2.1 \mu s$ and $1.7 \mu s$ for films of Pheo and $F_{64}PcZn$, respectively, indicate that Pheo in the lipid film is relatively less accessible to oxygen which could indicate that Pheo is incorporated into a lipid structure. It is likely that the preparation method of the films also influences the PS microenvironment which causes the appearance of lipid, self-organized structures such as micelles, in case of Pheo, as suggested by deviations of the 1O_2 luminescence signals from the fitted model for homogenous environments. Without further proof of the effective micro-environment, however, a better theoretical model cannot be proposed.

The generally shorter equilibrium PS triplet decay times in the pig ear, compared to the lipid films, indicates that the surrounding environment of the PS in skin is relatively more accessible by oxygen. This is due to several differences. For example, the lipid films are placed on a glass surface which hinders oxygen access from one side. In addition, the structure of the lipids, in the lipid-only film, is more compact compared to that of lipids in the skin where they occupy only the intercellular space.

3.6 Singlet Oxygen Generation in the Keratinous Component of Pig Ear Skin

Samples of the keratinous residue, prepared with $F_{64}PcZn$, exhibit 1O_2 luminescence. The time-resolved signals, however, could not be fit with the biexponential model due to the low signal intensity and, possibly, the presence of PS phosphorescence. Thus, a simplifying approach was employed to model the 1O_2 luminescence intensity. Specifically, the intensities were averaged over the first $20 \mu s$ after the laser pulse and the last $10 \mu s$ within the measurement time window of $80 \mu s$ after excitation. The difference obtained by subtracting the average intensity of the last $10 \mu s$ from the average intensity of the first $20 \mu s$ was attributed to a “short-lived” luminescence signal. The average value of the last $10 \mu s$ forms a long-lived intensity component. The change of the signal intensity of the short lived component, Fig. 11, reveals that this signal almost vanishes upon N_2 flushing of the sample chamber. Complete oxygen removal cannot be achieved, thus, a small signal may remain. Thus, a luminescence emission with a lifetime below $20 \mu s$ appears which suggests that a 1O_2 signal is emitted from the sample. The relatively short lifetime of $20 \mu s$ also indicates that the detected 1O_2 is not decaying in air where it could live up to hours.

Quantification of the long lived component suggests that this long-lived luminescence may be due to the phosphorescence of the PS. The intensity of this component increases under N_2 flushing and is not spectrally centred at 1270 nm . It can also be detected at 1200 nm where the short lived component

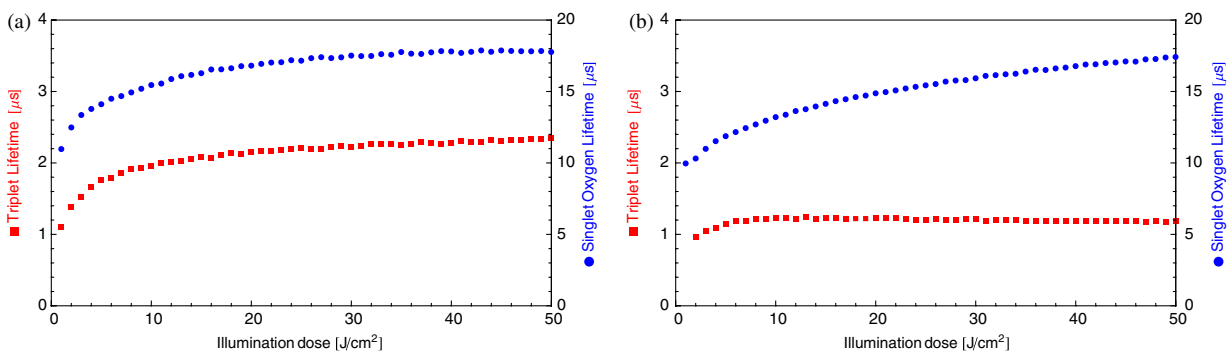


Fig. 10 Variation of singlet oxygen and photosensitizer triplet decay times in a film of subcutaneous tissue lipid as a function of light dose (the scale is proportional to a time scale of 0 to 7 min). The photosensitizer is (a) Pheo and (b) $F_{64}PcZn$ Fitted parameters: (a) initial measurement: $\tau_T = 1.0 \pm 0.2 \mu s$, $\tau_{O_2} = 11 \pm 0.5 \mu s$, final measurement (20 J/cm^2): $\tau_T = 2.1 \pm 0.2 \mu s$, $\tau_{O_2} = 18 \pm 0.5 \mu s$. (b) initial measurement $\tau_T = 0.9 \pm 0.2 \mu s$, $\tau_{O_2} = 11 \pm 0.5 \mu s$, final measurement: $\tau_T = 1.1 \pm 0.2 \mu s$, $\tau_{O_2} = 17 \pm 0.5 \mu s$.

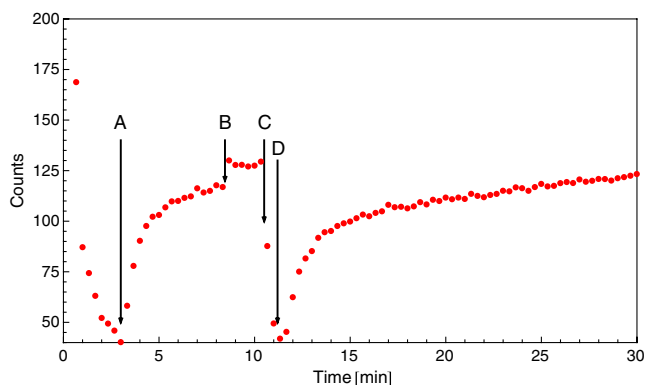


Fig. 11 Signal intensity of a short lived luminescence from keratinous scraps obtained from pig-ear stratum corneum prepared with $F_{64}PcZn$. The sample was flushed with N_2 from the beginning to point A. After A until point B air was allowed to re-enter the sample. At point B the sample was briefly flushed with compressed air. Between B and C the sample was exposed to normal atmosphere. This was followed by flushing with N_2 in the time between points C and D. After that the sample was exposed to normal atmosphere again. A signal intensity loss and recovery is observed under N_2 and exposure to air, respectively.

disappears. A possible 1O_2 emission in air is outshined by the phosphorescence.

In the case of Pheo 1O_2 luminescence signals remain below the system's sensitivity limit. The changes in the amplitude of the short lived component under change of atmosphere, in comparison to the long lived component, indicate that no 1O_2 emission can be tracked in this system. Also, no phosphorescence can be identified. Due to the preparation procedure, Pheo is present in the sample. However, when it dries out, it aggregates and the aggregates neither fluoresce nor produce 1O_2 .⁴⁸ The keratin has no ability to cause the monomerization of Pheo. In conclusion, the sample is not producing 1O_2 .

In contrast, $F_{64}PcZn$ cannot form aggregates and, thus, 1O_2 production remains possible in dry condition. The short lived component is, therefore, caused by 1O_2 which is quenched. Possible quenchers may either be keratin, which can be oxidized, or residual quenchers present within the keratinous residue.⁴⁴

3.7 Correlation Between Photosensitizer Localization and Singlet Oxygen Luminescence Kinetics

The complexity of skin composition prompted us to investigate the generation site of 1O_2 within the stratum corneum. The intercellular lipids are mainly organized as a lamellar system within a keratinous structure of high complexity.⁴⁹ Cellular membranes, in general, constitute a major accumulation site for Pheo in living cells *in vitro*.^{36,40} Considering the lipid structure of the intercellular lipids of the stratum corneum, as proposed previously, the incorporation of Pheo in this structure is likely even though the structure and composition of the lipid membranes in cells are different from the structure of the intercellular lipids.⁵⁰

Since fluorescence microscopy cannot reveal the PS localization within this ultrastructure of the stratum corneum, the isolation of the skin's major components was undertaken. The lipids from the stratum corneum were extracted as well the keratinous residue. Even though 1O_2 production in hair may occur, hair itself has not been further investigated here, as our studies are aimed at eventual PDT tumour treatment and, thus, focus on PS effects within the skin.⁵¹ Lipids from the tissue below the

stratum corneum were also extracted and investigated as $F_{64}PcZn$ was found there as well. The residue of the deeper layers was not investigated as these layers comprise viable cells which are severely affected by the lipid extraction procedure. All extracted lipids show 1O_2 emission when prepared with any of the PS. From samples of the keratinous residue, 1O_2 luminescence is observed only for $F_{64}PcZn$. This means, in case of pheo, only the intercellular lipids can serve as generation site for 1O_2 within the stratum corneum.

Skin samples treated with Pheo show a faster increase of the 1O_2 decay time with illumination at the beginning of the measurement, however, only a very slow rise after illumination with $20 J/cm^2$ light dose. In contrast, samples treated with $F_{64}PcZn$ show a slower increase in 1O_2 decay time which still rises even after a light dose of $20 J/cm^2$. The samples prepared with $F_{64}PcZn$ generally exhibit shorter 1O_2 decay times compared to those prepared with Pheo. In equal micro-environments (the volume that can be affected by 1O_2 via diffusion), this would result in a faster increase of decay time with illumination dose for the $F_{64}PcZn$ samples. As this is not observed, the micro-environments of the two PS must differ.

For the skin samples, several explanations can be used to model this behavior. Initially, the diffusion length of 1O_2 is limited. In a purely lipid system, 100 nm have been reported.⁴¹ This value may be an upper limit for the investigated systems. After consumption of chemical quencher within the micro-environment, physical quenching determines the equilibrium value of the 1O_2 decay time. The amount of chemical quenchers available for oxidation is limited to those within the micro-environment. Due to its chemical properties, $F_{64}PcZn$ is distributed more evenly. Thus, the overall amount of quenchers available for oxidation is larger compared to the membrane-incorporable Pheo. For Pheo, the micro-environment spans only the lipid structures. Therefore, the 1O_2 decay time of the Pheo samples more quickly reach an equilibrium state.

Secondly, $F_{64}PcZn$ is generating 1O_2 below the stratum corneum as well. Thus, the affected volume of the skin is also larger on a macro scale. Consequently, the affected skin volume of the $F_{64}PcZn$ samples contains a higher total amount of quenchers which offers more reaction sites for 1O_2 and decreasing the rate of change of rise and decay times with illumination.

Thirdly, the luminescence kinetics and 1O_2 generation loci are in good agreement considering the typical water concentration profile in the epidermis.⁵² At the junction between stratum corneum and the deeper layers of viable cells, the water content shows a sharp rise. The higher water content, in this environment, could explain the shorter 1O_2 decay time obtained in $F_{64}PcZn$ samples since water is an efficient physical quencher. The luminescence signals were fit biexponentially despite the fact that this is valid only in a homogenous environment. The additional generation of 1O_2 , with a short decay time in the layer of viable cells, would result in a lower fitting parameter for the decay time of the simple model. This explains the lower fitting parameter for the 1O_2 decay time of the $F_{64}PcZn$ sample compared to the Pheo sample where the 1O_2 is generated only in the stratum corneum. Due to the physical quenching by water, the rate of chemical quenching is reduced.

A quantification of the contribution of the respective factors is difficult. Nevertheless, the characteristic difference in change of the 1O_2 luminescence rise and decay times is also observed in the lipid extracts even though these are structurally very different systems. For the lipids especially, the possibility of the

formation of different microenvironments within the lipids can cause differences in the behavior of the two PSs, thus, making the first explanation the most likely one.

4 Conclusions and Prospects

Second to none, the $^1\text{O}_2$ luminescence in tissue was detected time-resolved using low excitation energies of 1 J/cm^2 per measurement. Using a compositional formulation similar to that used for topical PS application in clinics, two PSs, an amphiphilic one, Pheo and a highly hydrophobic one, F_{64}PcZn have been applied to pig ear skin.

A consistent picture of the PS localisation and its microenvironment can be presented. The amphiphilic Pheo generates $^1\text{O}_2$ only in the stratum corneum. The hydrophobic F_{64}PcZn was found to generate $^1\text{O}_2$ in the stratum corneum and as well in deeper layers of the epidermis, below the stratum corneum. Furthermore, lipids extracted from the epidermis show $^1\text{O}_2$ emission when prepared with any of the PS. From samples of the keratinous residue, $^1\text{O}_2$ luminescence is observed only for F_{64}PcZn . In consideration of the fluorescence measurements for Pheo, only the intercellular lipids can serve as generation site for $^1\text{O}_2$ within the stratum corneum. In contrast, $^1\text{O}_2$ generation within the corneocytes cannot be excluded for F_{64}PcZn .

Considerations of the $^1\text{O}_2$ luminescence decay times and their dependence on illumination dose give further conclusions about the microenvironment of the PS. Samples prepared with Pheo show a faster increase of $^1\text{O}_2$ luminescence decay time with increasing illumination dose. In comparison, samples prepared with F_{64}PcZn exhibit a slower increase. For the membrane-incorporable Pheo, the oxidation of local quenchers occurs at a higher rate which is likely due to the closer vicinity to the quencher molecules. This is not given for samples prepared with F_{64}PcZn . The distribution of F_{64}PcZn is more diffuse. This leads to a model for the microenvironment of the PSs within the ultrastructure of the stratum corneum: Pheo is incorporated into lipid structures formed by the intercellular lipids. In contrast, F_{64}PcZn is distributed more evenly and does not provoke the formation of a structured microenvironment.

The low excitation energies are crucial to reveal the kinetics of PS triplet state decay as well as that of $^1\text{O}_2$ under PDT relevant conditions. These times depend on the used PS and reflect the different accumulation loci and the PS microenvironment. We show that the light-dose induced variations of the decay times, after high illumination doses, also differ for both PSs which indicates different equilibrium values.

The described experimental and technical conditions demonstrate the possibility to use the time-resolved $^1\text{O}_2$ luminescence detection as a diagnostic tool. Light-dose induced variations of the luminescence kinetics can be tracked at light levels commonly applied for PDT treatment. Monitoring the $^1\text{O}_2$ interaction with tissue and the O_2 saturation level facilitates the improvement of clinical protocols for treatment and reduces stress for patients. Differences in PS efficacy, due to accumulation properties, can be assessed using $^1\text{O}_2$ luminescence detection. This provides an expeditious way to examine newly designed PS for their applicability in PDT.

Acknowledgments

The authors would like to thank Prof. J. Lademann from the Charité Berlin for supplying pig-ear samples and Heike Richter for carrying out the biopsies. We also thank Hans Scholz, head of the electronics workshop of the Institute of Physics and

Steffen Fahnauer and Michael Löbe from the mechanical workshop. We also thank Norbert Klose from Hamamatsu Germany. Hemantbhai Patel and Sergiu M. Gorun thank the US Army for financial support.

References

1. W. Baumler et al., "UVA and endogenous photosensitizers—the detection of singlet oxygen by its luminescence," *Photochem. Photobiol. Sci.* **11**(1), 107–117 (2012).
2. J. Baier et al., "Singlet oxygen by uva exposure of endogenous photosensitizers," *Biophys. J.* **91**(4), 1452–1459 (2006).
3. H. Masaki, "Role of antioxidants in the skin: anti-aging effects," *J. Dermatol. Sci.* **58**(2), 85–90 (2010).
4. A. Mahns et al., "Contribution of UVB and UVA to UV-dependent stimulation of cyclooxygenase-2 expression in artificial epidermis," *Photochem. Photobiol. Sci.* **3**(3), 257–262 (2004).
5. S. Grether-Beck et al., "Activation of transcription factor ap-2 mediates uva radiation and singlet oxygen-induced expression of the human intercellular adhesion molecule 1 gene," *Proc. Natl. Acad. Sci. U.S.A.* **93**(25), 14586–14591 (1996).
6. G. Kick et al., "Strong and prolonged induction of c-jun and c-fos proto-oncogenes by photodynamic therapy," *Br. J. Cancer* **74**(1), 30–36 (1996).
7. R. S. Cavalcante et al., "A combination of techniques to evaluate photodynamic efficiency of photosensitizers," *Laser Phys. Lett.* **6**(1), 64–70 (2009).
8. G. F. Vile and R. M. Tyrrell, "UVA radiation-induced oxidative damage to lipids and proteins *in vitro* and in human skin fibroblasts is dependent on iron and singlet oxygen," *Free Radic. Biol. Med.* **18**(4), 721–730 (1995).
9. M. C. DeRosa and R. J. Crutchley, "Photosensitized oxygen and its applications," *Coord. Chem. Rev.* **233–234**, 351–371 (2002).
10. J. C. Kennedy, R. H. Pottier, and D. C. Pross, "Photodynamic therapy with endogenous protoporphyrin ix: basic principles and present clinical experience," *J. Photochem. Photobiol. B* **6**(1–2), 143–148 (1990).
11. M. Niedre, M. S. Patterson, and B. C. Wilson, "Direct near-infrared luminescence detection of singlet oxygen generated by photodynamic therapy in cells *in vitro* and tissues *in vivo*," *Photochem. Photobiol.* **75**(4), 382–391 (2002).
12. J. R. Kanofsky, "Measurement of singlet-oxygen *in vivo*: progress and pitfalls," *Photochem. Photobiol.* **87**(1), 14–17 (2011).
13. Y. Y. Tian et al., "Mitochondria-involved apoptosis induced by mppa mediated photodynamic therapy," *Laser Phys. Lett.* **5**(10), 746–751 (2008).
14. R. W. Redmond and I. E. Kochevar, "Spatially resolved cellular responses to singlet oxygen," *Photochem. Photobiol.* **82**(5), 1178–1186 (2006).
15. J. Baier et al., "Time-resolved investigations of singlet oxygen luminescence in water, in phosphatidylcholine, and in aqueous suspensions of phosphatidylcholine or HT29 cells," *J. Phys. Chem. B* **109**(7), 3041–3046 (2005).
16. J. W. Snyder et al., "Optical detection of singlet oxygen from single cells," *Phys. Chem. Chem. Phys.* **8**(37), 4280–4293 (2006).
17. A. Jimenez-Banzo et al., "Kinetics of singlet oxygen photosensitization in human skin fibroblasts," *Free Radic. Biol. Med.* **44**(11), 1926–1934 (2008).
18. T. Herrling, K. Jung, and J. Fuchs, "Measurements of UV-generated free radicals/reactive oxygen species (ROS) in skin," *Spectrochim. Acta A Mol. Biomol. Spectrosc.* **63**(4), 840–845 (2006).
19. C. Flors et al., "Imaging the production of singlet oxygen *in vivo* using a new fluorescent sensor, Singlet Oxygen Sensor Green," *J. Exp. Bot.* **57**(8), 1725–1734 (2006).
20. A. Gollmer et al., "Singlet oxygen sensor green(R): photochemical behavior in solution and in a mammalian cell," *Photochem. Photobiol.* **87**(3), 671–679 (2011).
21. M. J. Niedre et al., "Singlet oxygen luminescence as an *in vivo* photodynamic therapy dose metric: validation in normal mouse skin with topical amino-levulinic acid," *Br. J. Cancer* **92**(2), 298–304 (2005).
22. M. J. Niedre et al., "Imaging of photodynamically generated singlet oxygen luminescence *in vivo*," *Photochem. Photobiol.* **81**(4), 941–943 (2005).

23. S. Lee et al., "A singlet molecular oxygen imaging sensor for photodynamic therapy," in *Biomedical Optics, OSA Technical Digest (CD)*, Optical Society of America, paper BTuC4 (2008).
24. C. Schweitzer and R. Schmidt, "Physical mechanisms of generation and deactivation of singlet oxygen," *Chem Rev* **103**(5), 1685–1757 (2003).
25. J. Baier et al., "Direct detection of singlet oxygen generated by UVA irradiation in human cells and skin," *J. Invest. Dermatol.* **127**(6), 1498–1506 (2007).
26. S. Lee et al., "A singlet oxygen monitor as an *in vivo* photodynamic therapy dosimeter," in *SPIE D. H. Kessel, Ed.*, pp. 738046–738049, SPIE, San Jose (2009).
27. S. Hackbarth et al., "New insights to primary photodynamic effects—Singlet oxygen kinetics in living cells," *J. Photochem. Photobiol. B* **98**(3), 173–179 (2010).
28. J. Schlothauer et al., *In vivo detection of time-resolved singlet oxygen luminescence under PDT relevant conditions*, D. H. Kessel, Ed., p. 755106, SPIE, San Francisco (2010).
29. J. Schlothauer, S. Hackbarth, and B. Röder, "A new benchmark for time-resolved detection of singlet oxygen luminescence—revealing the evolution of lifetime in living cells with low dose illumination," *Laser Phys. Lett.* **6**(3), 216–221 (2009).
30. U. Jacobi et al., "Porcine ear skin: an *in vitro* model for human skin," *Skin Res. Technol.* **13**(1), 19–24 (2007).
31. A. Willstätter and R. Stoll, *Untersuchungen über Chlorophyll*, Springer, Berlin (1913).
32. R. Gerdes et al., "Rational design of a reactive yet stable organic-based photocatalyst," *Dalton Trans.* **7**(7), 1098–1100 (2009).
33. J. Zimmermann et al., "Determination of the electron transfer parameters of a covalently linked porphyrin-quinone with mesogenic substituents—optical spectroscopic studies in solution," *J. Photochem. Photobiol. B* **40**(3), 209–217 (1997).
34. V. Kassis and J. Sondergaard, "Heat-separation of normal human skin for epidermal and dermal prostaglandin analysis," *Arch. Dermatol. Res.* **273**(3–4), 301–306 (1982).
35. M. Breternitz et al., "Acute barrier disruption by adhesive tapes is influenced by pressure, time and anatomical location: integrity and cohesion assessed by sequential tape stripping. A randomized, controlled study," *Br. J. Dermatol.* **156**(2), 231–240 (2007).
36. A. Paul et al., "Comparative study on the photosensitization of jurkat cells *in vitro* by Pheophorbide-a and a pheophorbide-a diaminobutane poly-propylene-imine dendrimer complex," *Laser Phys.* **13**(1), 22–29 (2003).
37. J. Baier et al., "Theoretical and experimental analysis of the luminescence signal of singlet oxygen for different photosensitizers," *J. Photochem. Photobiol. B* **87**(3), 163–173 (2007).
38. J. Schlothauer, "Zeitaufgelöster Nachweis von Singulett-Sauerstoff," pp. 49–55, Technische Universität Berlin, Berlin (2009).
39. A. A. Krasnovsky et al., "Photophysical Studies of pheophorbide-a and pheophytin-a phosphorescence and photo-sensitized singlet oxygen luminescence," *J. Photochem. Photobiol. B* **5**(2), 245–254 (1990).
40. B. Röde et al., "Photophysical properties of pheophorbidea in solution and in model membrane systems," *J. Porphyrins Phthalocyanines* **4**(1), 37–44 (2000).
41. B. Ehrenberg, J. L. Anderson, and C. S. Foote, "Kinetics and yield of singlet oxygen photosensitized by hypericin in organic and biological media," *Photochem. Photobiol.* **68**(2), 135–140 (1998).
42. B. A. Bench et al., "Introduction of bulky perfluoroalkyl groups at the periphery of zinc perfluorophthalocyanine: chemical, structural, electronic, and preliminary photophysical and biological effects," *Angew. Chem. Int. Ed. Engl.* **41**(5), 747–750 (2002).
43. R. Minnes et al., "Enhanced acidity, photophysical properties and liposome binding of perfluoroalkylated phthalocyanines lacking C-H bonds," *Photochem. Photobiol.* **82**(2), 593–599 (2006).
44. J. J. Thiele et al., "Protein oxidation in human stratum corneum: susceptibility of keratins to oxidation *in vitro* and presence of a keratin oxidation gradient *in vivo*," *J. Invest. Dermatol.* **113**(3), 335–339 (1999).
45. J. J. Thiele, "Oxidative targets in the stratum corneum. A new basis for antioxidative strategies," *Skin Pharmacol. Appl. Skin Physiol.* **14**(Suppl. 1), 87–91 (2001).
46. R. Dedic et al., "Singlet oxygen quenching by oxygen in tetraphenylporphyrin solutions," *J. Lumin.* **119**, 209–213 (2006).
47. S. H. White, D. Mirejovsky, and G. I. King, "Structure of lamellar lipid domains and corneocyte envelopes of murine stratum corneum. An X-ray diffraction study," *Biochemistry* **27**(10), 3725–3732 (1988).
48. B. Röder and H. Wabnitz, "Investigation on hematoporphyrin, mesoporphyrin, pheophorbide a and chlorin e6 in ethanol and aqueous solution by time-resolved fluorescence spectroscopy," *J. Photochem. Photobiol. B* **1**(1), 103–113 (1987).
49. L. Norlen, "Stratum corneum keratin structure, function and formation—a comprehensive review," *Int. J. Cosmet. Sci.* **28**(6), 397–425 (2006).
50. J. R. Hill and P. W. Wertz, "Molecular models of the intercellular lipid lamellae from epidermal stratum corneum," *Biochim. Biophys. Acta* **1616**(2), 121–126 (2003).
51. O. Chiarelli-Neto et al., "Generation and suppression of singlet oxygen in hair by photosensitization of melanin," *Free Radic. Biol. Med.* **51**(6), 1195–1202 (2011).
52. R. R. Warner, M. C. Myers, and D. A. Taylor, "Electron probe analysis of human skin: determination of the water concentration profile," *J. Invest. Dermatol.* **90**(2), 218–224 (1988).